

On the quaternary association of the type III secretion system HrcQ_B-C protein: Experimental evidence differentiates among the various oligomerization models

Vasiliki E. Fadouloglou^{a,b}, Marina N. Bastaki^a, Alison E. Ashcroft^c, Simon E.V. Phillips^c,
Nicholas J. Panopoulos^{a,d}, Nicholas M. Glykos^{b,*}, Michael Kokkinidis^{a,d,*}

^a Department of Biology, University of Crete, P.O. Box 2208, GR-71409 Heraklion, Crete, Greece

^b Department of Molecular Biology and Genetics, Democritus University of Thrace, Alexandroupolis, Greece

^c Astbury Centre for Structural Molecular Biology, School of Biochemistry and Molecular Biology, University of Leeds, Leeds LS2 9JT, UK

^d Institute of Molecular Biology and Biotechnology, P.O. Box 1527, GR-71110 Heraklion, Crete, Greece

ARTICLE INFO

Article history:

Received 28 October 2008

Received in revised form 16 January 2009

Accepted 25 January 2009

Available online 4 February 2009

Keywords:

Plant pathogens

Protein oligomerization state

Small-angle X-ray scattering (SAXS)

Circular dichroism (CD)

FliN protein

ABSTRACT

The HrcQ_B protein from the plant pathogen *Pseudomonas syringae* is a core component of the bacterial type III secretion apparatus. The core consists of nine proteins widely conserved among animal and plant pathogens which also share sequence and structural similarities with proteins from the bacterial flagellum. Previous studies of the carboxy-terminal domain of HrcQ_B (HrcQ_B-C) and its flagellar homologue, FliN-C, have revealed extensive sequence and structural homologies, similar subcellular localization, and participation in analogous protein–protein interaction networks. It is not clear however whether the similarities between the two proteins extend to the level of quaternary association which is essential for the formation of higher-order structures within the TTSS. Even though the crystal structure of the FliN is a dimer, more detailed studies support a tetrameric donut-like association. However, both models, dimer and donut-like tetramer, are quite different from the crystallographic elongated dimer of dimers of the HrcQ_B-C. To resolve this discrepancy we performed a multidisciplinary investigation of the quaternary association of the HrcQ_B-C, including mass-spectrometry, electrophoresis in non-reductive conditions, gel filtration, glutaraldehyde cross-linking and small angle X-ray scattering. Our experiments indicate that stable tetramers of elongated shape are assembled in solution, in agreement with the results of crystallographic studies. Circular dichroism data are consistent with a dimer–dimer interface analogous to the one established in the crystal structure. Finally, molecular dynamics simulations reveal the relative orientation of the dimers forming the tetramers and the possible differences from that of the crystal structure.

© 2009 Published by Elsevier Inc.

1. Introduction

Type III secretion system (TTSS)¹ is a protein traffic device used by several plant and animal pathogenic bacteria for injecting virulence factors directly into the eukaryotic cytosol (Hueck, 1998). It is viewed as a ‘molecular syringe’ composed by an elongated extracellular, needle-like structure and a cylindrical base which is embed-

ded into the two bacterial membranes and ends in a cytoplasmic extension. Low resolution electron microscopy data (He and Jin, 2003; Kubori et al., 1998; Sekiya et al., 2001; Tamano et al., 2000) showed that TTSSs from different pathogens share a common structure and that TTSS and flagellar hook–basal body complex are quite similar. The most prominent architectural similarities are observed between the TTSS cylindrical base and the flagellar basal body. They are both multiprotein complexes assembled by highly symmetrical substructures each of which is constructed by multiple copies of a protein or of a protein complex. In terms of their amino acid sequences, these proteins are broadly conserved among all known TTSSs and the flagellum and they constitute the so called conserved core (Buttner and Bonas, 2002, 2003; Rossier et al., 1999; Tampakaki et al., 2004).

HrcQ_B is a conserved protein from the TTSS of the plant pathogen *Pseudomonas syringae* pv. phaseolicola. Genetic and biochemi-

* Corresponding authors. Fax: +30 25510 30613 (N.M. Glykos), +30 2810 394351 (M. Kokkinidis).

E-mail addresses: glykos@mbg.duth.gr (N.M. Glykos), kokkinid@imbb.forth.gr (M. Kokkinidis).

¹ Abbreviations: TTSS, type III secretion system; SDS–PAGE, sodium dodecyl sulphate–polyacrylamide gel electrophoresis; DTT, 1,4-dithiothreitol; ESI-MS, electrospray ionization mass spectrometry; SAXS, small-angle X-ray scattering; CD, circular dichroism; UV, ultraviolet; rmsd, root mean squared deviation; rms, root mean squared.

cal experiments have shown (Fadouloglou et al., 2004) that the protein is located at the cytoplasmic site of the inner bacterial membrane, interacts with at least one other protein of TTSS (the HrcQ_A protein) and this interaction is mainly established *via* its highly conserved carboxy-terminal domain. The crystal structure of the conserved C-terminal domain, residues 50–128 (hereafter referred to as HrcQ_{B-C}), has been determined to a resolution of 2.3 Å (Fadouloglou et al., 2004). In the crystals, HrcQ_{B-C} forms an elongated, gently curved homo-tetramer. Two monomers fold together in a symmetrical manner to form a compact and highly intertwined dimeric structure (Fig. 1A). Two dimers are packed together to form a dimer of dimers (Fig. 1B). The flagellar homologue of HrcQ_B, FliN protein, has been extensively studied and experimental observations which concern its subcellular localization and protein–protein interactions are fully consistent with properties of HrcQ_B (Francis et al., 1994; Mathews et al., 1998; Tang et al., 1995; Zhao et al., 1996). Thus, both proteins are mainly located in the cytoplasm and they adopt a similar pattern of protein–protein interactions. For example, the HrcQ_B interacts with the HrcQ_A protein and the analogous interaction has also been reported between the flagellar FliN and the, HrcQ_A-analogue, FliM protein. Moreover, it has been shown (Zhao et al., 1996) that FliN is a major component of the cytoplasmic extension of the basal body, called the C-ring. In addition, Spa33, the HrcQ_B homologue from *Shigella*, has also shown to be an essential C-ring (Morita-Ishihara et al., 2006) component. Even though there is no direct experimental evidence for the existence of the C-ring in plant pathogens, the extensive similarities between HrcQ_B, FliN and Spa33 do suggest that the TTSS of plant pathogens may include a cytoplasmic structure analogous to flagellar C-ring. In that case, it would be difficult to predict the extent of the structural correspondence. However, it seems rational to presume that the HrcQ_B would participate in this ring as a major building block. The hypothesis of functional and structural analogies between HrcQ_B and FliN was strengthened by the crystal structure determination (Brown et al., 2005) of the conserved C-terminal domain of the FliN (hereafter referred to as FliN-C), residues 68–154 (1yab.pdb) or residues 59–154 (1o6a.pdb) which revealed similar tertiary structure with HrcQ_{B-C} (the C_α-rmsd for 138 residues is 2 Å, and 1.1 Å if surface loops are excluded).

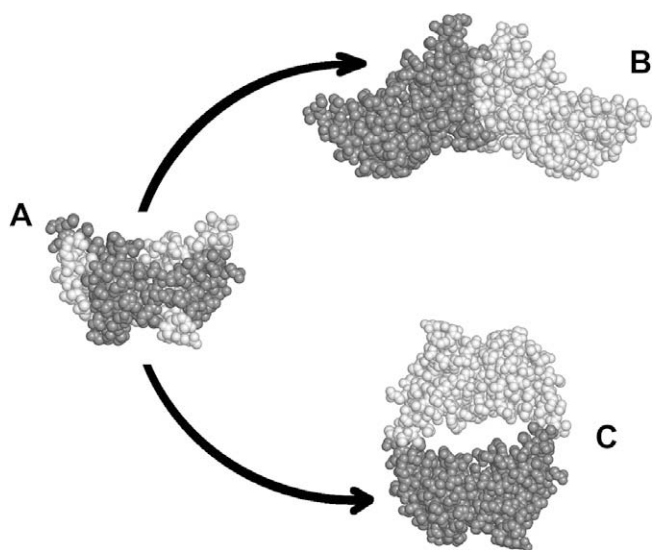


Fig. 1. Possible oligomerization states of the HrcQ_{B-C} protein. (A) The dimer. (B) The elongated tetramer (dimer of dimers) found in the crystals of the protein. (C) A donut-like tetramer formed accordingly to the model proposed for the FliN-C.

Except from the similarities mentioned above the two proteins might have also significant functional differences. Thus, for example, it has been shown that FliN is related with the flagellar motility and that it is closely involved in the process of the direction switching, functions which could not have correspondence to the injectisomes. At the present, it remains unclear whether HrcQ_B and FliN are organized into similar quaternary associations, which is a critical property for the formation of higher-order structures. Given the functional differences, the possibility of important structural differences at the level of quaternary association is particularly valid. The crystal structure of HrcQ_{B-C} revealed a homo-tetrameric dimer of dimers (Fig. 1B) while FliN-C from *Thermotoga maritima* is a dimer, roughly equivalent to a HrcQ_{B-C} dimer (Fig. 1A), both in crystals and in solution (Brown et al., 2005). On the other hand, in analytical ultracentrifugation experiments the FliN protein from *Escherichia coli* behaved as a tetramer with a shape factor indicating an elongated shape (Brown et al., 2005) in agreement with the HrcQ_{B-C} model. However, more recent biochemical/mutagenesis data for the *E. coli* FliN have been interpreted as being consistent with a donut-like homo-tetrameric association (Paul and Blair, 2006). A hypothetical donut-like association for the HrcQ_{B-C} is shown in Fig. 1C.

In the present study, we investigate the solution quaternary association of the HrcQ_{B-C} protein from *P. syringae* pv. phaseolicola and compare our results with existing models for the FliN proteins. For this purpose we used a variety of biochemical, biophysical and computational techniques i.e. SDS–polyacrylamide gel electrophoresis (SDS–PAGE), cross-linking by glutaraldehyde, size–exclusion chromatography, mass spectroscopy, mutagenesis, circular dichroism, small angle X-ray scattering and molecular dynamics simulations. Our results suggest (i) a tetrameric association with the overall dimensions and the elongated shape of the crystallographic HrcQ_{B-C} tetramer and (ii) a probable rearrangement of the dimers with consequences on the interface area.

2. Materials and methods

2.1. Overexpression and purification

HrcQ_{B-C} was overexpressed and purified as described earlier (Fadouloglou et al., 2001). The I41W-G74W mutant of HrcQ_{B-C} was produced by PCR reactions using the appropriate sets of primers according to the method described by Fisher and Pei (1997). The gene of the full length HrcQ_B was initially mutated and the isoleucine residue corresponding to Ile 41 of the HrcQ_{B-C} was changed to Trp in the first PCR reaction. The template in this PCR was the *hrcQ_B* gene in the vector pT7-7 and the primers which were used were: upper (mutagenesis primer) 5'-tggCTTGAAGTCACCGG CATTTCGC-3', lower 5'-AGTCCCGGCATCTAGACGGCGCAGTTCGG-3'. The mutation site is indicated by the lowercase letters. The lower primer contains a XbaI restriction site, which is underlined. The final product from the first PCR was used as the template of a second PCR for the production of the I41W mutant of *hrcQ_{B-C}*. The primers used were: upper 5'-CAGCGCAGGATCCACAGGACG AGCCC-3', lower 5'-CAAGAAACAGCGCCAGGATCCTCGG-3'. The BamHI fragment (BamHI restriction sites is underlined) was cloned into the vector pPROEX-HTa. For the final construct a third PCR followed. The I41W mutant of *hrcQ_{B-C}* in the pPROEX-HTa vector was used as template. The primers were: upper 5'-CAGATTACC CGCCTGGTGACCCGA-3', lower 5'-CAGccaCAGGCGACCCTCGACATC CACCAG-3'. The mutation site is indicated by the lowercase letters. The PstI fragment (PstI restriction sites is underlined) was cloned into the vector pPROEX-HTa and then the pPROEX-HTa/I41W-G74W-*hrcQ_{B-C}* plasmid was used to transform DH5 *E. coli* cells. Mutation was confirmed by restriction digestion and sequencing.

The I41W-G74W mutant of HrcQ_B-C protein was purified following the protocol used for the native HrcQ_B-C (Fadouloglou et al., 2001).

2.2. Size-exclusion chromatography and glutaraldehyde cross-linking

Size-exclusion chromatography was carried out using a Sephacryl S-100 column (Pharmacia) previously equilibrated with 20 mM Tris/HCl pH 7.5, 50 mM NaCl, 2 mM DTT at 294 K. The column was calibrated with the low molecular weight calibration kit from Amersham Biosciences containing bovine serum Albumin (molecular weight of 67 kDa, Stokes radius of 35.5 Å), hen egg Ovalbumin (43 kDa, 30.5 Å), bovine pancreas Chymotrypsinogen A (25 kDa, 20.9 Å) and bovine pancreas Ribonuclease A (13.7 kDa, 16.4 Å). Elution was monitored by measuring absorption at 230 nm because the absence of aromatic side chains results in weak peaks at 280 nm.

Cross-linking studies of the protein's oligomerization state were performed as described (Fadouloglou et al., 2008). In summary, 15 µl of protein sample (0.5 mg/ml purified HrcQ_B-C in 50 mM phosphate buffer, pH 8.0) was placed on a cover slip which was used to seal a chamber containing 40 µl of 25% v/v glutaraldehyde. The protein solution, which formed a hanging drop inside the chamber, was exposed to glutaraldehyde's vapours for varying time intervals at 303 K and subsequently was mixed with an equal volume of 2× SDS-PAGE loading buffer and analysed by SDS-PAGE.

2.3. Mass spectrometry

Electrospray ionization (ESI) mass-spectrometry (MS) was carried out using a benchtop single quadrupole mass spectrometer (Platform II, Micromass UK Ltd.). For "native" electrospray conditions the protein was extensively dialyzed against 20 mM NH₄HCO₃ pH 8.0 adjusted by acetic acid and filtered. The final sample concentration was approximately 1 mg/ml (1 pmol/µl assuming dimers) estimated by the Bradford method (Bradford, 1976). When "denaturing" electrospray conditions were used, the sample was analysed in 0.05% aqueous formic acid and methanol (1:1). In both cases positive ionization electrospray was used. Data were acquired over the *m/z* range 770–1880 for the "native" and 500–1900 for the "denaturing" conditions. The spectra were transformed to a molecular-mass scale using maximum entropy techniques (Ferrige et al., 1992). Horse heart myoglobin (molecular mass 16951.5 Da from Sigma Chemical Co.) was used for external calibration to ensure mass accuracy.

2.4. Small-angle X-ray scattering data acquisition and analysis

Small-angle X-ray scattering (SAXS) data of HrcQ_B-C were collected at the European Molecular Biology Laboratory on the X33 beamline of the Deutsches Elektronen-Synchrotron (DESY, Hamburg). Scattering curves were measured at protein concentrations of 1.9, 3.7, 5.6, 8.4, 12.6 and 25.2 mg/ml estimated by absorption at 280 nm assuming an extinction coefficient of 250 M⁻¹ cm⁻¹. The solvent was 20 mM Tris/HCl pH 7.5, 50 mM NaCl. The sample temperature was stable at 285 K, the exposure time was 2 min per measurement and the data were collected on an image plate detector Mar345. With the sample to detector distance at 2.4 m and the X-ray wavelength (λ) adjusted at 1.5 Å the range of momentum transfer which was covered is $0.08 < s < 4.5 \text{ nm}^{-1}$ (where $s = 4\pi \sin \theta / \lambda$, 2θ is the scattering angle). Repetitive exposures of the same protein solution indicated no changes in the scattering pattern and thus no measurable radiation damage of the samples. All the data processing and analysis steps were performed using the program package ATSAS (Kozin and Svergun, 2001; Svergun, 1992, 1999; Svergun et al., 1995; Volkov and Svergun, 2003). The

scattering of the buffer was subtracted from the scattering of the solution and the difference curves extrapolated to infinite dilution using the program PRIMUS (Konarev et al., 2003). This procedure generates a scattering curve which is assumed to be free from interparticle interference. The distance distribution function $p(r)$ was calculated using the program GNOM (Svergun, 1992) and from that the maximum particle size D_{max} was estimated and shape information was obtained. CRY SOL (Svergun et al., 1995) was used for calculation of scattering curves for the three atomic models shown in Fig. 1. The radius of gyration R_g was calculated using the Guinier approximation (Guinier, 1939) and the distance distribution function. Particle shape was also calculated from the SAXS data using the *ab initio* procedure implemented in DAMMIN (Svergun, 1999). The calculations were conducted first without imposing any symmetry or shape constraints and later assuming 2-fold symmetry and a prolate shape for the molecular envelope. The generated models were averaged by DAMAVER (Volkov and Svergun, 2003). The high resolution crystal structure of HrcQ_B-C (1o9y.pdb) and the *ab initio* shape data obtained by DAMMIN program were superimposed using SUPCOMB (Kozin and Svergun, 2001).

2.5. Circular dichroism data and protein thermostability

Circular dichroism spectra and temperature-dependent protein unfolding profiles were measured with a Peltier temperature-controlled Jasco J-810 spectrometer. The protein samples (0.1–0.3 mg/ml for far UV measurements and 1 mg/ml for near UV measurements) were in 10 mM phosphate buffer at pH 7.5. The far UV spectra (190–250 nm) were measured in quartz cells of 0.1 cm optical pathlength, and represent an average of three accumulations. Spectra were acquired at a scan speed of 10 or 20 nm min⁻¹ and a response time of 4 or 2 s, respectively. The near UV spectra (260–320 nm) were collected in cells of 0.5 cm pathlength and represent an average of three accumulations. Spectra were acquired at a scan speed of 20 nm min⁻¹ and a response time of 2 s. All spectra were corrected for the buffer baseline.

Proteins were subjected to the thermal melting profile by monitoring the changes of the circular dichroism spectra at 203 and 289 nm. Temperature of the samples was continuously varied from 25 to 95 °C with a constant rate of 0.7 °C/min.

2.6. Molecular dynamics simulation and data analysis

Starting from the crystallographically determined coordinates of the HrcQ_B-C (entry 1o9y.pdb), missing side chains and hydrogen atoms were built with PSFGEN from the NAMD distribution (Kale et al., 1999). The molecule was solvated using VMD (Humphrey et al., 1996) in an orthogonal box of pre-equilibrated TIP3 water (Jorgensen et al., 1983) with dimensions $130 \times 76 \times 64 \text{ \AA}^3$. The charge of the solute was neutralized through the addition of sodium and chloride ions to a final concentration of 100 mM. The final system comprised 4356 protein atoms, 55,038 water atoms and 36 ions (28 sodium and 8 chloride ions). The molecular dynamics simulations were performed with the program NAMD v.2.5 (Kale et al., 1999) using the CHARMM22 force field (MacKerell et al., 1998) as follows. The system was first energy minimized for 4 ps with the positions of all backbone atoms fixed and then for another 4 ps without positional restraints. It was then heated from 0 K to the target temperature of 320 K over a period of 12 ps with the positions of C α atoms harmonically restrained about their energy minimized positions. Subsequently, the system was equilibrated for 200 ps under NpT conditions without any restraints. This was followed by the production NpT run which lasted for 42 ns with the temperature and pressure controlled using the Nosé-Hoover Langevin dynamics and Langevin piston barostat control methods

as implemented by NAMD program and maintained at 320 K and 1 atm. Periodic boundary conditions were imposed and all atoms were wrapped to the nearest image. The production run was performed with the impulse Verlet-I multiple-time step integration algorithm as implemented by NAMD. The inner time step was 2 fs. Short-range nonbonded interactions were calculated every two steps and long-range electrostatic interactions every four time steps using the particle mesh Ewald method (Darden et al., 1993). All bonds involving hydrogen atoms were constrained by the SHAKE algorithm. A switching function was employed at 10 Å and van der Waals potential energy was smoothly truncated at 12 Å. The number of grid points for the fast Fourier transformations was 128, 80, 64 for the *x*, *y*, *z* directions, respectively. Trajectories were obtained by saving the atomic coordinates of the whole system every 0.4 ps. Calculations and analysis were performed with the programs CARMA (Glykos, 2006), X-PLOR (Brünger, 1992) and locally written software. Cluster analysis of the trajectory was performed by the statistical analysis program R.

2.7. Homology modelling

The coordinates of donut-like FliN-C (kindly provided by Prof. D. Blair) were used for obtaining the donut-like model of HrcQ_B-C.

This model was produced by two successive least squared superposition runs of the HrcQ_B-C dimer onto the two dimers of the FliN-C which form the donut structure. Superpositions were performed by the program LSQKAB (Kabsch, 1978). It is worth mentioning that some N-terminal interfacial residues are absent from the HrcQ_B-C donut because the HrcQ_B-C structure does not include them due to their high flexibility. However, the corresponding N-terminal residues are present in the FliN-C structure and contribute to the dimer–dimer interface of the FliN donut.

3. Results and discussion

3.1. The basic building unit of the HrcQ_B-C is the crystallographic dimer

The molecular mass of the HrcQ_B-C protein was primarily investigated by ESI-MS. Under “native” electrospray ionization conditions (20 mM NH₄HCO₃ pH 8.0) the molecular mass profiles generated by the *m/z* spectra (Fig. 2A) indicate a single, homogeneous population of particles with a molecular weight of 17,886.2 ± 1.2 Da. Under “denaturing” conditions at pH ~ 3 the spectrum was again dominated by a component of the same molecular weight (17,885.1 ± 0.4 Da) and its quality was indicative of a high level of purity (data not shown).

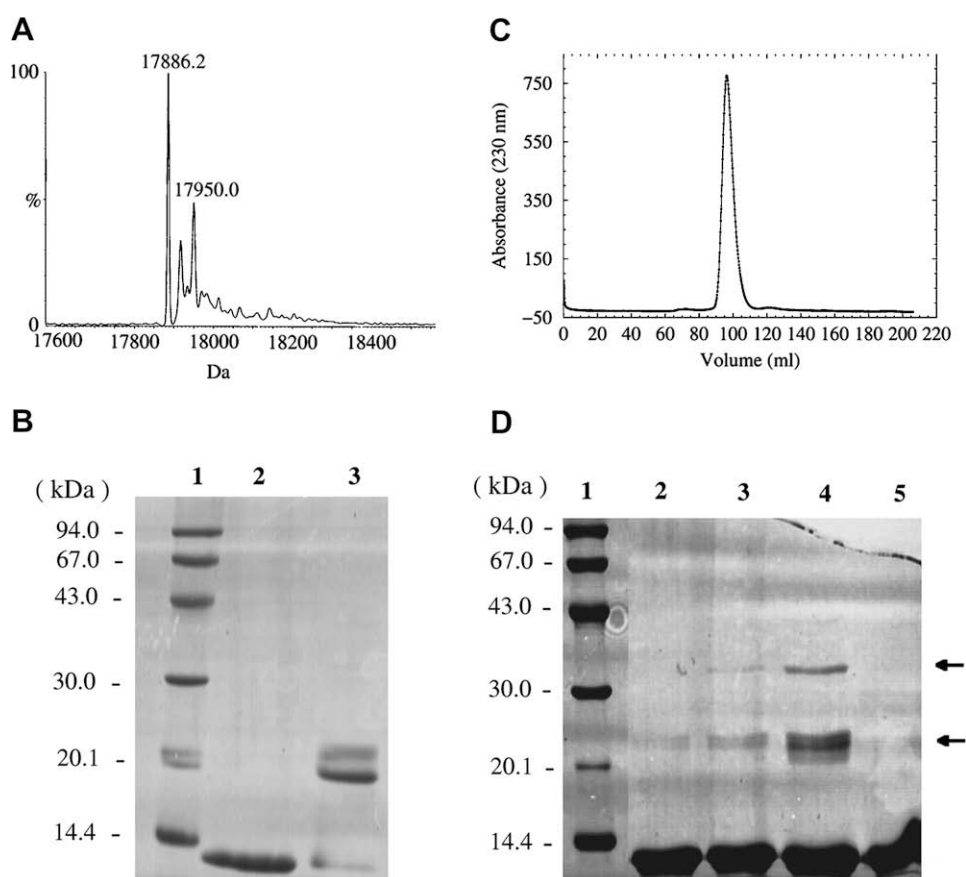


Fig. 2. The HrcQ_B-C forms oligomeric assemblies. (A) ESI-MS of purified HrcQ_B-C. The molecular mass profile generated by maximum entropy processing of the *m/z* spectrum shows essentially one major component of molecular mass 17,886.2 Da. The major component is accompanied by less intense species at 17,917.6 and 17,950.0 Da, ~32 and 64 (=2 × 32) Da higher in mass. It is possible that this species may be adducts of the protein with amide ions (16 Da) produced from the solvent (NH₄HCO₃). (B) SDS-PAGE, 15% Laemmli of the HrcQ_B-C protein in the presence and absence of reducing agent. Lane 1: low molecular weight marker. Lane 2: sample of the protein which was heated at 90 °C in the presence of β-mercaptoethanol. The sample runs as monomers (the molecular weight of monomers is approximately 8.9 kDa). Lane 3: Sample of the protein which was heated at 90 °C in the absence of β-mercaptoethanol. The majority of the protein runs as a double band to a molecular weight of approximately 20 kDa clearly indicating the presence of dimers. (C) Gel filtration studies of HrcQ_B-C. Shephacryl S-100 gel filtration column chromatography is shown. The protein is eluted in a volume which is consistent with either a spherical pentamer or an elongated tetramer. (D) Glutaraldehyde cross-linking of the HrcQ_B-C. SDS-PAGE, 15% Laemmli. Lane 1: low molecular weight marker. Lane 5: the original sample without treatment with glutaraldehyde. Lanes 2–4: influence of the glutaraldehyde vapours on the protein solution for time intervals of 10, 20 and 60 min. The presence of a second and a third population with molecular weights of approximately 22 and 35 kDa (corresponding to dimers and tetramers) can be seen clearly in lane 4.

Since the theoretical molecular weight of the monomer is 8945 Da, a value of 17,886 is very close to the theoretical molecular weight of the dimer (17,890 Da) and shows that under the electrospray ionization conditions the sample is present in the form of dimers. We thus conclude that the smallest, stable structural unit of the protein is the dimer. Because the dimer remains intact even under denaturing conditions where the weak interactions—hydrogen bonds and van der Waals forces—are expected to be fully destroyed, we conclude that this dimer is probably stabilized by covalent bond(s).

To further investigate the kind of these bonds the protein sample was analysed by SDS–PAGE avoiding previous treatment with any reducing agent i.e. the SDS–PAGE loading buffer was prepared without addition of β -mercaptoethanol. As Fig. 2B (lane 3) shows the protein runs as a double band with an apparent molecular weight corresponding to that of a dimer. This indicates that two monomers are connected by one or more disulphide bonds.

The results from the spectrometric and electrophoretic experiments are consistent with and fully explained by the dimers of the crystallographically determined HrcQ_B-C structure. These dimers are stabilized by an extensive network of hydrogen bonds along a β -ribbon and also by a disulphide bridge entirely buried in the interior of the dimer. This S–S bridge is present even after treatment with 10 mM DDT. Thus, we conclude that the dimer identified by the mass spectra is the crystallographically determined dimer.

3.2. The HrcQ_B-C dimers can associate to form tetramers

Since the crystal structure showed that the protein forms tetrameric assemblies we tried to determine if a higher-order association of the HrcQ_B-C dimers is also present in solution. For this purpose cross-linking experiments by glutaraldehyde were carried out (Fadouloglou et al., 2008). After incubation for 60 min with vapours of glutaraldehyde, the cross-linked protein species were analysed using SDS–PAGE 15% Laemmli (Fig. 2D, lane 4) and showed

three bands corresponding to molecular weights of monomer, dimer and tetramer (approximately 10, 22 and 35 kDa). These results suggest that the protein does can form tetramers. The low yield of the cross-linking reaction, even after 60 min incubation, is possibly due to the complete absence of lysine residues (Lundblad and Noyes, 1984; Payne, 1973).

The oligomerization state of the protein in solution was further investigated by size-exclusion chromatography. For this purpose a Sephacryl S-100 column calibrated by the low molecular weight calibration kit of Pharmacia was used. Three runs were carried out using samples from different protein preparations as well as independently packed and calibrated columns. In all cases, the protein eluted as a single, sharp peak indicating a monodisperse molecular population (Fig. 2C). Assuming a spherical molecular envelope, the elution volume corresponds to a globular protein with an average estimated molecular weight of 42 kDa. This value is inconsistent with the presence of dimers (18 kDa) or hexamers ($3 \times$ dimer, $3 \times 18 = 54$ kDa). However, it fits well to a tetramer ($2 \times$ dimer, $2 \times 18 = 36$ kDa) of elongated shape. The average Stokes radius of the protein was also estimated by size-exclusion chromatography to be 28 Å. This value is in good agreement with the Stokes radius of the crystallographically determined tetramer, 29.1 Å (García-de-la-Torre et al., 2000) (the crystallographic dimer has a Stokes' radius of 21.9 Å). The crystallographically determined HrcQ_B-C tetramer is thus a good starting model for the protein in solution.

3.3. The low resolution structure of HrcQ_B-C in solution is a crystal-like, elongated tetramer

To further explore the quaternary association of HrcQ_B-C in solution we performed a series of SAXS experiments. The data were compared with scattering patterns calculated from the atomic models of: (i) the HrcQ_B-C dimer (Fig. 1A), (ii) the crystal-like tetramer (Fig. 1B) and (iii) a donut-like tetramer (Fig. 1C), which have been proposed for the FlhN-C (Paul and Blair, 2006). For the analysis

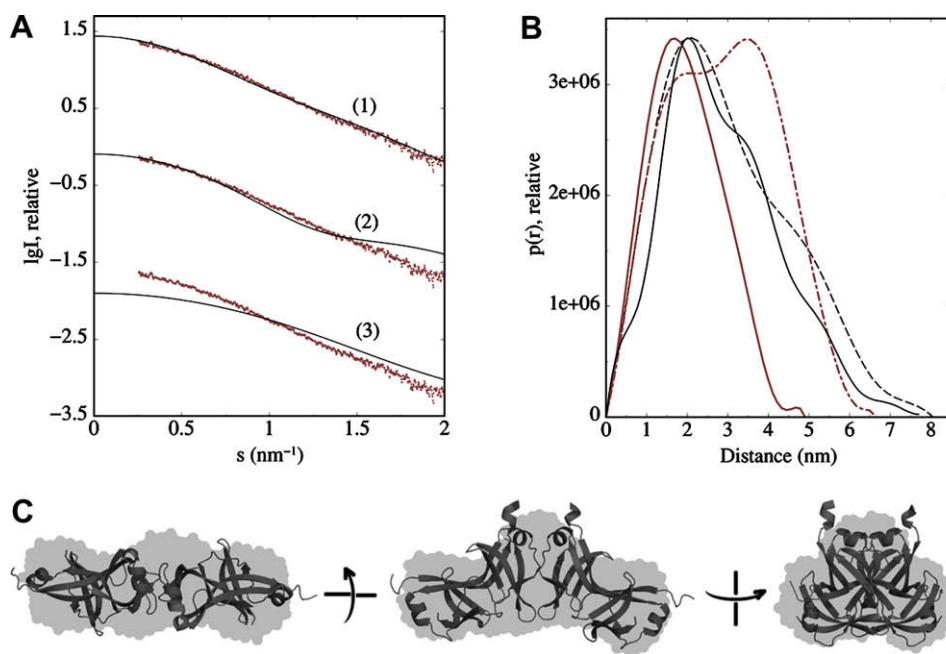


Fig. 3. SAXS data for the HrcQ_B-C indicate an elongated shape resembling the crystal-like tetramer. (A) Experimental scattering data (points) are compared with the scattering curves computed from the three models i.e. the crystal-like tetramer (curve 1), the donut-like tetramer (curve 2) and the dimer (curve 3). The curves (2) and (3) are displaced down by one logarithmic unit for clarity. (B) The experimental distance distribution function (continuous line, $D_{\max} \sim 8$ nm) is compared with calculated distance distribution functions for the crystal-like tetramer (dashed line) and the donut-like tetramer (dashed-dotted line). The calculated distance distribution function of the dimer is also shown for comparison (continuous line, $D_{\max} \sim 5$ nm). (C) Comparison between the molecular envelope calculated *ab initio* from SAXS data and the crystallographic tetramer. The agreement is illustrated by the fitting of the crystal structure as a ribbon diagram into the envelope constructed by SAXS data.

only the low resolution data ($s \leq 2 \text{ nm}^{-1}$) were used which include information for the overall shape of the scattering particle. As shown in Fig. 3A, the best agreement between experimental and calculated (from the three models mentioned above) data is achieved with the crystal-like tetramer. The scattering curve which is calculated from the crystal structure essentially coincides with the low resolution experimental data. On the other hand, both the donut-like tetramer and the dimer significantly deviate from the experimental data almost along the full range of resolution examined. These data in accordance with the results of the preceding section clearly exclude the dimer as the possible oligomer of the HrcQ_B-C in solution.

The dimer significantly differs from the other two models both with respect to its shape and also its size and so was readily excluded as a possible oligomerization state. On the other hand, the crystal-like and donut-like structures have similar sizes and their distinction can only be based on their different shapes using e.g. the distance distribution function $p(r)$ (Svergun, 1992). Fig. 3B shows the experimental distance distribution function of our protein which has the typical profile of an elongated particle. In the same graph the calculated $p(r)$ of the crystallographic and donut-like tetramers as well as of the dimer are presented for comparison. Taking this procedure one step further, the overall shape of the protein was predicted *ab initio* (Svergun, 1999; Volkov and Svergun, 2003) and it is presented in Fig. 3C. The molecular envelope which was reconstructed by these calculations further supports the model of an elongated tetramer. The resemblance with the crystallographic structure is illustrated by the superposition of the crystal structure with the envelope obtained by the SAXS data.

Size-exclusion chromatography and SAXS data support an elongated particle shape which is in agreement with the shape of the crystallographically determined structure of the HrcQ_B-C. However, it is possible that the dimers in this particle are oriented in different manner compared to the crystallographic structure leading to a different dimer–dimer interface. To explore this possibility, two residues which are located on the surface of the dimer and directly involved in the formation of the crystallographic interface, Ile 41 and Gly 74, were replaced by Trp residues and the effects of these substitutions were monitored by size-exclusion chromatography and circular dichroism experiments. In particular, the hypothesis which is tested with the experiments described below is: If these positions (41 and 74) are also found in the interface of the solution tetramer then we expect that (i) Their replacement by a bulky Trp residue would force the dimers to adopt a different arrangement upon tetramer formation with subsequent effects on the hydrodynamic properties of the molecule possibly detectable by size-exclusion chromatography. Otherwise, if positions 41 and 74 are located on the surface of the solution tetramer, we expect that their occupation by another residue even as large as the tryptophan could not cause observable changes to the hydrodynamic properties. (ii) The side chains of tryptophans 41 and 74 would be inside or close to the hydrophobic environment of the interface having low mobility, adopting few, distinct conformations and giving thus rise to intense CD tryptophanyl bands at the near UV which would be appeared at wavelengths characteristic of the hydrophobic environment. Otherwise, if positions 41 and 74 are located on the surface of the solution tetramer we expect that tryptophan side chains would be exposed to the polar solvent and their

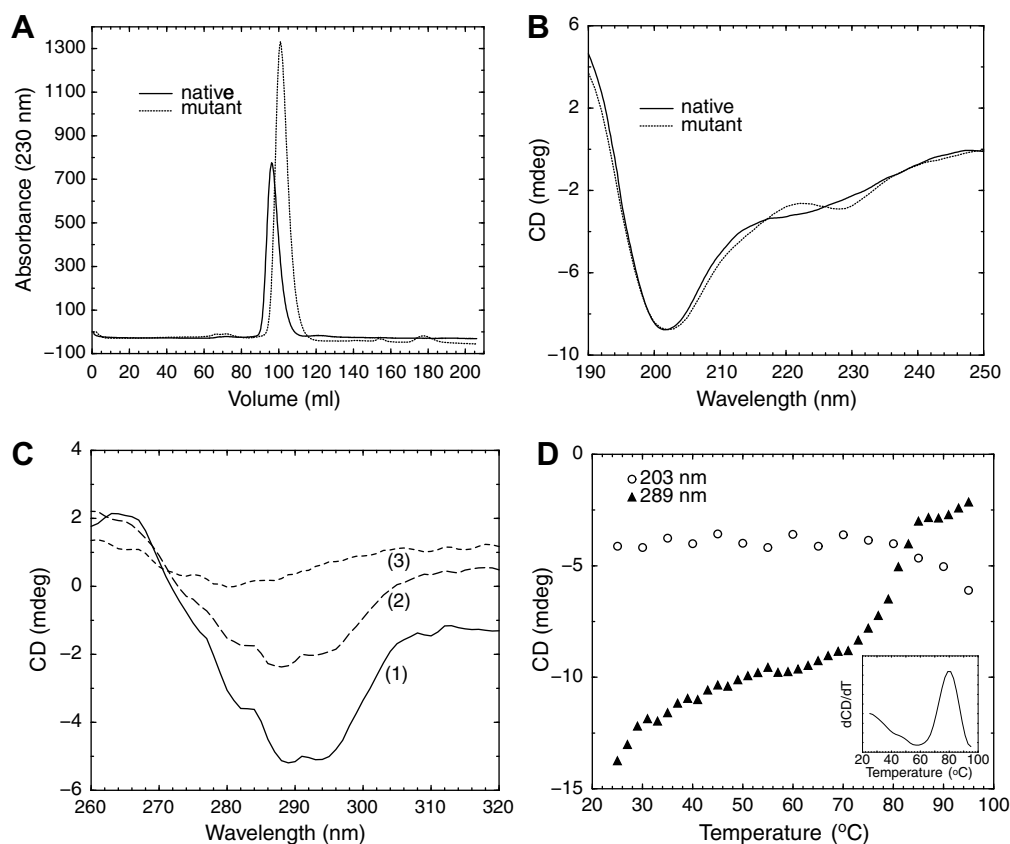


Fig. 4. Studies of a Trp double mutant provide clues for the location of the interface area. (A) Comparison of gel filtration chromatographs for native HrcQ_B-C (continuous line) and the I41W-G74W mutant (dotted line). The mutant protein is systematically eluted 5 ml after the native confirming the interference of the mutated residues on the overall shape/size of the molecule. (B) Comparison of far UV spectra for native HrcQ_B-C (continuous line) and I41W-G74W mutant (dotted line). Spectra are almost identical suggesting similar secondary structures. (C) Near UV spectra for I41W-G74W. Curve 1, spectrum of the protein at room temperature (25 °C). Curve 2, spectrum of acidified protein sample with HCl. Curve 3, spectrum of denatured at 95 °C protein sample. (D) Temperature scans for I41W-G74W at 203 nm (open circles) and 289 nm (filled triangles), which monitor alterations at secondary structure and the tryptophans' environment, respectively. Graph in insertion is the first derivative of the temperature scan at 289 nm.

high mobility would lead to tryptophanyl CD bands of low intensity.

I41W-G74W protein was overexpressed and purified to homogeneity in conditions similar to that used for the native molecule. In size-exclusion chromatography the mutant protein is eluted 5 ml after the native protein (reproducible result from two different protein preparations with independently packed and calibrated columns) and 14 ml ahead of the theoretically expected elution volume of the dimer (Fig. 4A). These results suggest a particle with Stokes radius 2 Å smaller than that of the native protein even though it appears to retain a tetrameric association. A decrease of the hydrodynamic radius as a result of the substitution of two small amino acids, Ile and Gly by the much bigger Trp residues clearly indicates that the experimental observations do not represent the effect of a simple amino acid exchange but probably reflect significant rearrangements occurring in the molecule. Given the position of the mutations, at the surface of the dimer, it is evident that they affect the dimer–dimer interactions associated with the formation of tetramers. Thus this observation is consistent with the hypothesis that positions 41 and 74 are found and/or in-

involved in the interface of the solution tetramer as they do in the crystallographic tetramer.

The far UV CD spectra of native and mutant proteins were similar and characteristic of the β_{II} class of proteins (Sreerama and Woody, 2003) with a prominent minimum at 202–203 nm and a smaller maximum around 188 nm (Fig. 4B). Comparison of the spectra indicates that the mutant protein fully retained the native secondary structure and thus that the mutations do not affect the overall secondary structure of the protein. The differences between the spectra could be assigned to minor structural alterations or even to a possible contribution of Trp residues to the far UV area (Pflumm and Beychok, 1969).

The near UV CD spectrum of the mutant protein (Fig. 4C) fully arises from the mutated Trp residues since the native HrcQ_{B-C} has no aromatic side chains. I41W-G74W has two tryptophans per protein chain. Assuming a quaternary structure analogous to the crystallographically determined tetramer we expect four out of the eight tryptophans to be solvent exposed thus having a high degree of mobility and a minor, if any, contribution to the near UV CD spectrum. The remaining four, due to the symmetrical organi-

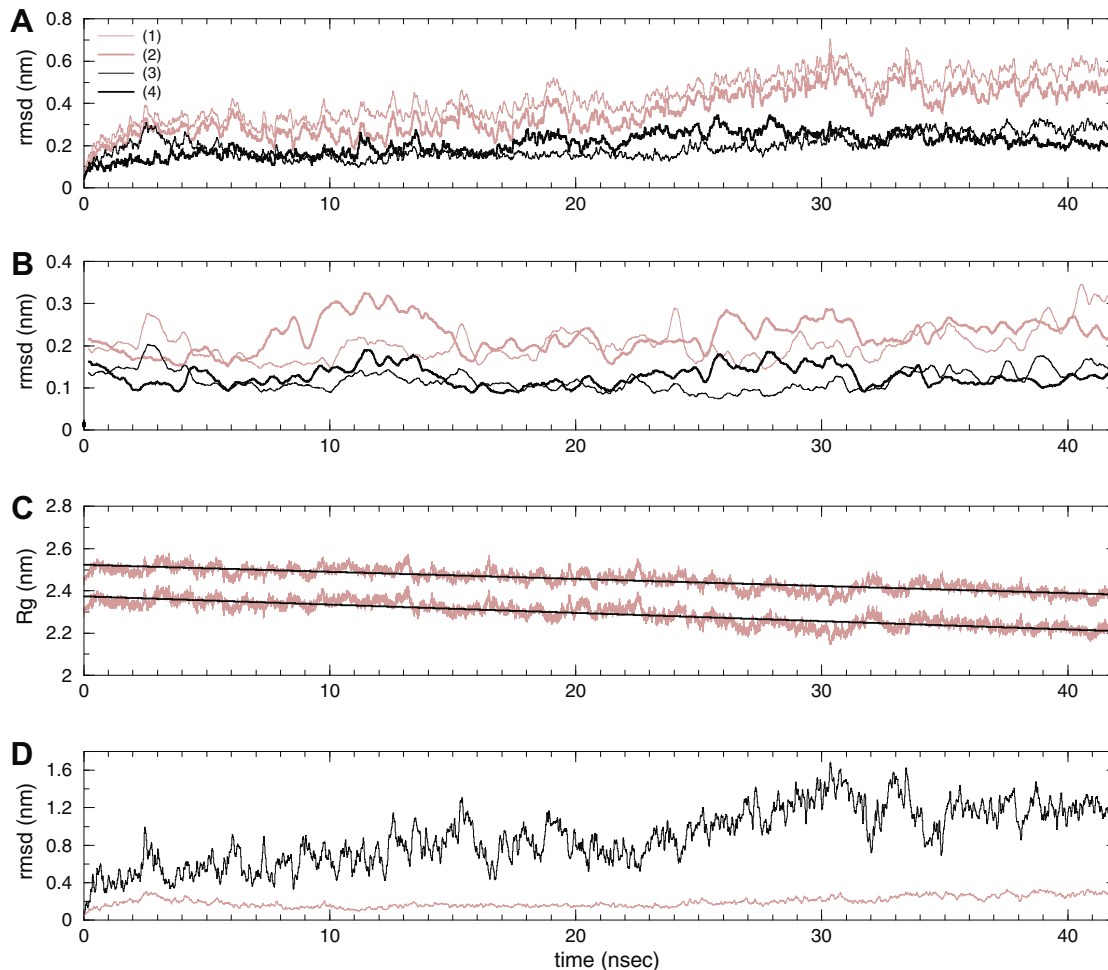


Fig. 5. The HrcQ_{B-C} crystal structure is stable but the dimers' relative orientation changes. (A) Brown line graphs represent the evolution of the C_α-rms deviation between the starting (crystal) tetrameric structure and each of the structures recorded during the simulation. For calculation of curves 1 and 2 the flexible terminal/loop residues included and excluded, respectively. Black line graphs represent the evolution of the C_α-rms deviation between the starting (crystal) structure of AD (curve 3) or BC (curve 4) dimers and each of their structures recorded during the simulation. For these calculations flexible terminal/loop residues have been excluded. (B) Evolution of the C_α-rms deviation between the simulation-derived average structures of AD (thin lines) or BC (bold lines) dimers and each of their structures recorded during this same simulation. For graphs represented by black lines flexible terminal/loop residues have been excluded. (C) Evolution of the value of the radius of gyration during the simulation for the whole tetramer (upper graph) and after excluding flexible terminal/loop residues (lower graph). (D) For this panel, the trajectory structures were superimposed using the BC dimer and then the evolution of C_α-rms deviation between the successive AD dimer structures was recorded (black line). In the same graph, the brown line shows, for reference, the C_α-rms deviation between the successive structures of the BC dimer. Flexible terminal/loop residues have been excluded from this calculation. (For interpretation of the references to color in this figure legend, the reader is referred to the web version of this article.)

graphic structure is relatively small and this deviation is getting even smaller if from the calculation the flexible parts of the structure are excluded. Fig. 5A, graphs 3 and 4, shows the C_{α} -rmsd of dimers AD and BC, respectively, after excluding flexible terminal/loop residues from the calculation. Both dimers converge within the first 5 ns and their structure remains stable and deviates in average between 2 and 2.5 Å from the starting structure for the following 37 ns. Second, the radius of gyration for each dimer is stable and fluctuates ± 0.5 Å around the initial value (data not shown). Third, the polypeptide chain not only remains folded, as the stable R_g value implies, but the secondary structure elements are con-

served as we can conclude by comparing the frequencies of the secondary structure elements of each chain with the secondary structure of the chains from the crystal structure. Fig. 6 compares the secondary structure element assignments for chain A in the crystal structure (upper panel) and during the simulation (lower panel). At the beginning of simulation each chain of the protein consists of a long β -strand, a short α -helix and three consecutive β -strands connected by turns. The overall secondary structure profile remains unchanged with all β -strands and the unique α -helix being preserved in the time scale of simulation. Lastly, each of the dimers converges to an average structure from which deviates

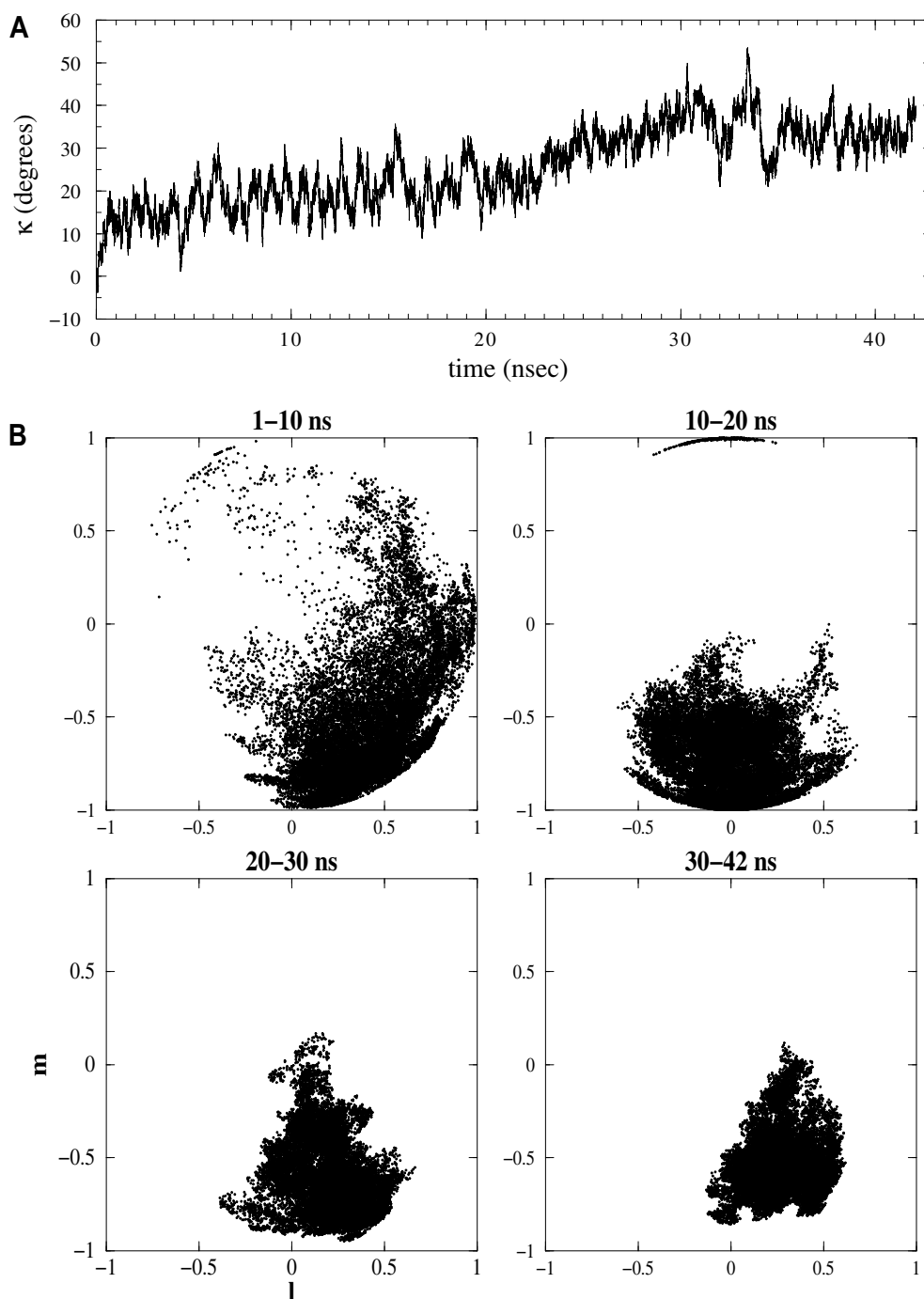


Fig. 7. Evolution of the relative orientation of AD dimer against its initial position. The rotation matrices which transform AD to its initial position for each frame of the trajectory have been converted to polar angles κ, ϕ, ω . (A) Evolution of the value of the rotation angle κ . (B) For clarity the trajectory has been divided into four time periods of 10 ns each. Dots represent the projection of the transformation axis, for each frame, onto the surface of a sphere (polar stereographic projections). l and m are direction cosines defined as $l = \sin \omega \cos \phi$ and $m = \sin \omega \sin \phi$.

by no more than 1.3 Å (see Fig. 5B, graphs represented by brown lines, thin for AD, bold for BC dimers) and by only 0.5 Å when the terminal/loop residues have been excluded from the calculation (see Fig. 5B, graphs represented by black lines, thin for AD, bold for BC dimers).

Comparing the plots presented in Fig. 5A and B we conclude that the high final rmsd value of the whole structure cannot be justified by the movements of the flexible termini/loops or the structural alterations occurring inside the dimers. Furthermore, Fig. 5C (upper graph) shows that during the simulation the R_g of the tetramer is slowly but steadily decreasing from an average starting value of 25.2 Å to the average value of 23.7 Å. The folding/unfolding and rearrangement of the N-termini could only partly account for this change since the R_g value decreases (from 23.7 to 22.1 Å) even after the exclusion of these termini from the calculation (Fig. 5C, lower graph). The rearrangement of the dimers relative to each other seems to be the main reason for the observed decrease of the R_g as well as for the significant (as judged by the rmsd measures) deviation from the initial structure. This can be quantified by superimposing the tetramer on the BC dimer only, and then calculating the evolution of C_α -rmsd of the AD dimer (Fig. 5D, black line). In that case the C_α -rmsd reaches the value of about 12 Å and seems to be stabilized only during the last 10 ns of simulation. These data imply a progressive alteration of the relative orientation between the dimers. This progressive rearrangement of dimers is clearly demonstrated by the polar stereographic projection graphs shown in Fig. 7B. Having superimposed the tetramer structure using only the BC dimer, the rotation matrix which transforms AD to its starting orientation is calculated for each and every frame of the trajectory. Then the rotations matrices are converted to polar angles ω , ϕ and κ (MacKerell et al., 1998). The evolution of the value of the rotation angle κ during the simulation is shown in Fig. 7A, while the evolution of the direction of the rotation axis is presented on the polar stereographic projections of Fig. 7B. It is evident from the inspection of Fig. 7B that at the beginning of simulation (1–10 ns) the dimer AD moves significantly with respect to its initial position. However, as the simulation progress the orientation of AD dimer falls in a small only cluster of the possible space and appears to converge to a position different than that determined by the crystal structure. This is also confirmed by cluster analysis of the trajectory which indicated two main clusters of structures. The one includes frames 1–85,199 (1–34 ns) and the other frames 85,200 to the last (34–42 ns).

The MD simulation reveals structural properties which are consistent with experimental observations. Thus, the simulation demonstrates a high mobility for the N-terminal ends as well as for some solvent exposed loop regions. These are parts of the crystallographic structure which do not fit inside the SAXS envelope as Fig. 3C shows. Moreover, according to SAXS data which estimate a smaller D_{max} than the model of crystal structure (Fig. 3B) the MD simulation also implies a decrease of the R_g value in comparison with the R_g of the starting crystal structure (Fig. 5C). Finally, the MD-derived structure (Fig. 8) explains better than the crystal structure the CD/mutagenesis data. As it is shown in Fig. 8, positions 41 and 74 are more exposed to the surface and the bulky tryptophanyl chains could be packed without to cause the dissociation of the tetramers. Moreover, the MD-derived structure provides a model which could explain the decrease of the Stoke's radius as a consequence of the substitution of two small amino acids by the much bigger Trp residues.

4. Conclusions

Extensive similarities between the HrcQ_B and its homologues FliN and Spa33 suggest that the TTSS of plant pathogens may in-

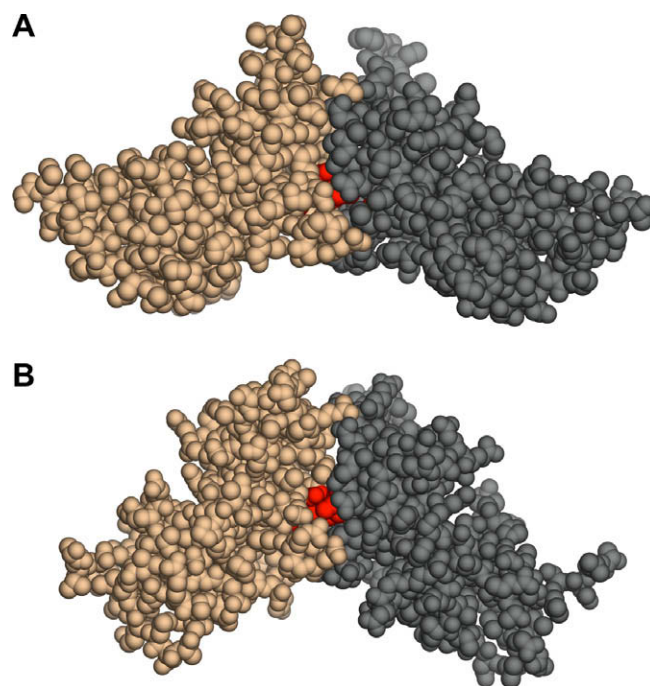


Fig. 8. Comparison of the crystallographically determined and the MD-derived HrcQ_B-C tetramers. Space filling representations of (A) the crystallographically determined HrcQ_B-C tetramer and (B) the MD-derived tetramer, which represents the average structure for the last 8 ns of simulation. The interfacial residues which have been mutated to tryptophans (see Section 3.3) are coloured red. (For interpretation of the references to color in this figure legend, the reader is referred to the web version of this article.)

clude a multiprotein, cytoplasmic complex analogous to the C-ring found in the flagellum and the TTSS of animal pathogens. The architecture and organization of this multiprotein assembly are open questions of great interest. Here, we investigate *in vitro* the quaternary association of the HrcQ_B-C protein which presumably constitutes an essential building block of the C-ring. We have used a variety of experimental and computational techniques to find evidence for the oligomeric association of the protein in solution and to validate the stability of this association. Our results are summarized as follows. Electrospray mass-spectrometry, SDS-polyacrylamide gel electrophoresis and crystallography converge to the conclusion that the protein in solution cannot be found in units smaller than the crystallographic dimers. Moreover, cross-linking experiments indicated the presence of assemblies greater than the dimer. Size-exclusion chromatography indicates a homogeneous population with the protein to form elongated tetramers consistently with the crystallographic structure. SAXS data also confirm an elongated molecular envelope inside which the crystal structure is nicely fitted. In addition, CD/mutagenesis data are consistent with the existence of tryptophan residues (positions 41 and 74) in buried or semi-buried positions of the quaternary association indicating for the solution tetramer an interface which could not be dramatically different than that of the crystal structure. Finally, in agreement with the previous findings, extensive molecular dynamics simulations confirmed the stability of a crystal-like tetramer and provided a model for the dimer-to-dimer arrangement which is slightly different from that of the crystal structure and fully explains the experimental observations.

Although our experiments provide solid evidence for the self-organization of the protein *in vitro*, however we cannot claim that the same homo-tetrameric association necessarily occurs within the cell where the HrcQ_B could preferably interact with other protein partners. This is particularly true given that the absence of

electron microscopy data from the cytoplasmic/inner-membrane parts of the plant pathogenic type III secretion systems makes impossible a comparison with our model.

However, the present study could be used as a useful guide to check the functional importance of this homo-tetrameric association *in vivo*. This could be done by designing and making mutations which would destabilize or fully destroy the dimer-to-dimer association and then measuring the functional consequences. For this purpose, it is worth mentioning that: (i) The elongated tetramer is highly stable so that it seems unlikely that a single, point mutation could be able to fully destroy it. This is especially true given that the I41W-G74W mutant is still a tetramer. (ii) The residues Ile 41, Val 67 and Val 69 participate in the formation of the hydrophobic interfacial core of the tetramer. We propose that the mutation of these residues to a highly polar one i.e. Asp or Glu could possibly dissociate or destabilize the dimer-to-dimer assembly.

This work establishes a useful foundation for further exploration of the organization of the HrcQ_B-C protein in the *P. syringae* type III secretion system. For example, a topic of great interest is to be found out what prevents further association of the dimers into larger, than the tetramers, assemblies. A rational hypothesis would be that the dimer-to-dimer association alters the conformation of the protein so that the outer-facing parts are altered and further end-to-end association is prevented. This hypothesis is consistent with the observed rms deviations within and between the dimers i.e. 0.79 and 0.75 Å within the dimers, 0.25 Å between the interfacial sites and 0.31 Å between the outer-facing parts. Further computational evidence is being sought by extensive molecular dynamics simulations.

Acknowledgments

We thank Prof. David Blair who made available to us the coordinates of the donut-like model of FlhN-C and Prof. D. Svergun who help us with SAXS data collection and analysis.

This work was partially supported by grants in the framework of PEP (KP-15) and the Greece-Bulgaria Joint Research and Technology Programmes 2004–2006 of GSRT. V.E.F. was supported by a Postdoctoral Research Fellowship from the Greek State Scholars' Foundation. We thank the EMBL/Hamburg Outstation and the EU for support through the EU-13 access grant from the EU Research Infrastructure Action under the FP6 "Structuring the European Research Area Programme", Contract No. RII3/CT/2004/5060008.

References

- Bradford, M.M., 1976. A rapid and sensitive method for the quantitation of microgram quantities of protein utilizing the principle of protein-dye binding. *Anal. Biochem.* 72, 248–254.
- Brown, P.N., Mathews, M.A.A., Joss, L.A., Hill, C.P., Blair, D.F., 2005. Crystal structure of the flagellar rotor protein FlhN from *Thermotoga maritima*. *J. Bacteriol.* 187, 2890–2902.
- Brünger, A.T., 1992. X-PLOR, version 3.1.
- Buttner, D., Bonas, U., 2002. Port of entry—the type III secretion translocon. *Trends Microbiol.* 10, 186–192.
- Buttner, D., Bonas, U., 2003. Common infection strategies of plant and animal pathogenic bacteria. *Curr. Opin. Plant Biol.* 6, 312–319.
- Darden, T., York, D., Pedersen, L., 1993. Particle mesh Ewald. An $N \log(N)$ method for Ewald sums in large systems. *J. Chem. Phys.* 98, 10089–10092.
- Fadouloglou, V.E., Kokkinidis, M., Glykos, N.M., 2008. Determination of protein oligomerization state: two approaches based on glutaraldehyde crosslinking. *Anal. Biochem.* 373, 404–406.
- Fadouloglou, V.E., Tampakaki, A.P., Panopoulos, N.J., Kokkinidis, M., 2001. Structural studies of the Hrp secretion system: expression, purification, crystallization and preliminary X-ray analysis of the C-terminal domain of the HrcQ_B protein from *Pseudomonas syringae* pv. phaseolicola. *Acta Crystallogr. D* 57, 1689–1691.
- Fadouloglou, V.E., Tampakaki, A.P., Glykos, N.M., Bastaki, M.N., Hadden, J.M., Phillips, S.E., Panopoulos, N.J., Kokkinidis, M., 2004. Structure of HrcQ_B-C, a conserved component of the bacterial type III secretion systems. *Proc. Natl. Acad. Sci. USA* 101, 70–75.
- Ferrige, A.G., Seddon, M.J., Green, B.N., Jarvis, S.A., Skilling, J., 1992. Disentangling electrospray spectra with maximum-entropy. *Rapid Commun. Mass Spectrom.* 6, 707–711.
- Fisher, C., Pei, G.K., 1997. Modification of a PCR-based site-directed mutagenesis method. *Biotechniques* 23, 570–574.
- Francis, N.R., Sosinsky, G.E., Thomas, D., DeRosier, D.J., 1994. Isolation, characterization and structure of bacterial flagellar motors containing the switch complex. *J. Mol. Biol.* 235, 1261–1270.
- García-de-la-Torre, J., Huertas, M.L., Carrasco, B., 2000. Calculation of hydrodynamic properties of globular proteins from their atomic-level structure. *Biophys. J.* 78, 719–730.
- Gasymov, O.K., Abduragimov, A.R., Yusifov, T.N., Glasgow, B.J., 2003. Resolving near-ultraviolet circular dichroism spectra of single trp mutants in tear lipocalin. *Anal. Biochem.* 318, 300–308.
- Glykos, N.M., 2006. Carma: a molecular dynamics analysis program. *J. Comput. Chem.* 27, 1765–1768.
- Guinier, A., 1939. La diffraction des rayons X aux très petits angles; application à l'étude de phénomènes ultramicroscopiques. *Ann. Phys. (Paris)* 12, 161–237.
- Gurd, F.R.N., Friend, S.H., Rothgeb, T.M., Gurd, R.S., Scouloudi, H., 1980. Electrostatic stabilization in sperm whale and harbor seal myoglobins. Identification of groups primarily responsible for changes in anchoring of the A helix. *Biophys. J.* 32, 65–75.
- He, S.Y., Jin, Q., 2003. The Hrp pilus: learning from flagella. *Curr. Opin. Microbiol.* 6, 15–19.
- Hueck, C.J., 1998. Type III protein secretion systems in bacterial pathogens of animals and plants. *Microbiol. Mol. Biol. Rev.* 62, 379–433.
- Humphrey, W., Dalke, A., Schulten, K., 1996. VMD: visual molecular dynamics. *J. Mol. Graph.* 14, 33–38.
- Jorgensen, W.L., Chandrasekhar, J., Madura, J.D., Impey, R.W., Klein, M.L., 1983. Comparison of simple potential functions for simulating liquid water. *J. Chem. Phys.* 79, 926–935.
- Kabsch, W., 1978. A solution for the best rotation to relate two sets of vectors. *Acta Crystallogr. A* 32, 922–923.
- Kale, L., Skeel, R., Bhandarkar, M., Brunner, R., Gursoy, A., Krawetz, N., Phillips, J., Shinozaki, A., Varadarajan, K., Schulten, K., 1999. NAMD2: greater scalability for parallel molecular dynamics. *J. Comput. Phys.* 151, 283–312.
- Konarev, P.V., Volkov, V.V., Sokolova, A.V., Koch, M.H.J., Svergun, D.I., 2003. PRIMUS: a Windows PC-based system for small-angle scattering data analysis. *J. Appl. Crystallogr.* 36, 1277–1282.
- Kozin, M.B., Svergun, D.I., 2001. Automated matching of high- and low-resolution structural models. *J. Appl. Crystallogr.* 34, 33–41.
- Kubori, T., Matsushima, Y., Nakamura, D., Uralil, J., Lara-Tejero, M., Sukhan, A., Galan, J.E., Aizawa, S.I., 1998. Supramolecular structure of the *Salmonella typhimurium* type III protein secretion system. *Science* 280, 602–605.
- Lundblad, R.L., Noyes, C.M., 1984. Chemical Reagents for Protein Modification. CRC Press, Boca Raton, FL.
- MacKerell, A.D., Bashford, D., Bellott, M., Dunbrack, R.L., Evanseck, J.D., Field, M.J., Fischer, S., Gao, J., Guo, H., Ha, S., Joseph-McCarthy, D., Kuchnir, L., Kuczera, K., Lau, F.T.K., Mattos, C., Michnick, S., Ngo, T., Nguyen, D.T., Prodhom, B., Reiher, W.E., Roux, B., Schlenkrich, M., Smith, J.C., Stote, R., Straub, J., Watanabe, M., Wiorkiewicz-Kuczera, J., Yin, D., Karplus, M., 1998. All-atom empirical potential for molecular modelling and dynamics studies of proteins. *J. Phys. Chem. B* 102, 3586–3616.
- Mathews, M.A., Tang, H.L., Blair, D.F., 1998. Domain analysis of the FlhM protein of *Escherichia coli*. *J. Bacteriol.* 180, 5580–5590.
- Morita-Ishihara, T., Ogawa, M., Sagara, H., Yoshida, M., Katayama, E., Sasakawa, C., 2006. Shigella Spa33 is an essential C-ring component of type III secretion machinery. *J. Biol. Chem.* 281, 599–607.
- Paul, K., Blair, D.F., 2006. Organization of FlhN subunits in the flagellar motor of *Escherichia coli*. *J. Bacteriol.* 188, 2502–2511.
- Payne, J.W., 1973. Polymerization of proteins with glutaraldehyde. *Biochem. J.* 153, 867–873.
- Pflumm, M.N., Beychok, S., 1969. Optical activity of cystine-containing proteins. II. Circular dichroism spectra of pancreatic ribonuclease A, ribonuclease S, and ribonuclease S-protein. *J. Biol. Chem.* 244, 3973–3981.
- Rossier, O., Wengelnik, K., Hahn, K., Bonas, U., 1999. The *Xanthomonas* Hrp type III system secretes proteins from plant and animal bacterial pathogens. *Proc. Natl. Acad. Sci. USA* 96, 9368–9373.
- Sekiya, K., Ohishi, M., Ogino, T., Tamano, K., Sasakawa, C., Abe, A., 2001. Supermolecular structure of the enteropathogenic *Escherichia coli* type III secretion system and its direct interaction with the EspA-sheath-like structure. *Proc. Natl. Acad. Sci. USA* 98, 11638–11643.
- Sreerama, N., Woody, R.W., 2003. Structural composition of β_I - and β_{II} -proteins. *Protein Sci.* 12, 384–388.
- Strickland, E.H., Horwitz, J., Billups, C., 1969. Fine structure in the near-ultraviolet circular dichroism and absorption spectra of tryptophan derivatives and chymotrypsinogen A at 77 degrees K. *Biochemistry* 8, 3205–3213.
- Strickland, E.H., Horwitz, J., Kay, E., Shannon, L.M., Wilchek, M., Billups, C., 1971. Near-ultraviolet absorption bands of tryptophan. Studies using horseradish peroxidase isoenzymes, bovine and horse heart cytochrome c, and N-stearyl-L-tryptophan *n*-hexyl ester. *Biochemistry* 10, 2631–2638.
- Svergun, D.I., 1992. Determination of the regularization parameter in indirect-transform methods using perceptual criteria. *J. Appl. Crystallogr.* 25, 495–503.
- Svergun, D.I., 1999. Restoring low resolution structure of biological macromolecules from solution scattering using simulated annealing. *Biophys. J.* 76, 2879–2886.

- Svergun, D.I., Barberato, C., Koch, M.H.J., 1995. CRY SOL—a program to evaluate X-ray solution scattering of biological macromolecules from atomic coordinates. *J. Appl. Crystallogr.* 28, 768–773.
- Tamano, K., Aizawa, S.-I., Katayama, E., Nonaka, T., Imajoh-Ohmi, S., Kuwae, A., Nagai, S., Sasakawa, C., 2000. Supramolecular structure of the *Shigella* type III secretion machinery: the needle part is changeable in length and essential for delivery of effectors. *EMBO J.* 19, 3876–3887.
- Tampakaki, A.P., Fadouloglou, V.E., Gazi, A.D., Panopoulos, N.J., Kokkinidis, M., 2004. Conserved features of type III secretion. *Cell. Microbiol.* 6, 805–816.
- Tang, H., Billings, S., Wang, X., Sharp, L., Blair, D.F., 1995. Regulated underexpression and overexpression of the FliN protein of *Escherichia coli* and evidence for an interaction between FliN and FliM in the flagellar motor. *J. Bacteriol.* 177, 3496–3503.
- Volkov, V.V., Svergun, D.I., 2003. Uniqueness of *ab initio* shape determination in small-angle scattering. *J. Appl. Crystallogr.* 36, 860–864.
- Zhao, R., Pathak, N., Jaffe, H., Reese, T.S., Khan, S., 1996. FliN is a major structural protein of the C-ring in the *Salmonella typhimurium* flagellar basal body. *J. Mol. Biol.* 261, 195–208.